

# Mo-Si-B Alloy Development

## J. H. Schneibel

Oak Ridge National Laboratory, Metals and Ceramics Division, P. O. Box 2008, Oak Ridge, TN 37831-6115

E-mail: schneibeljh@ornl.gov; Telephone: (865) 576-4644; Fax: (865) 574-7659

## Jamie J. Kruzic

Lawrence Berkeley National Laboratory, 1 Cyclotron Road, Berkeley, CA 94720, U.S.A.

Email: jjkruzic@lbl.gov; Telephone: (510) 486-5544; Fax: (510) 486-4995

## Robert O. Ritchie

Lawrence Berkeley National Laboratory, 1 Cyclotron Road, Berkeley, CA 94720, U.S.A.

Email: roritichie@lbl.gov; Telephone: (510) 486-5798; Fax: (510) 486-4881

## ABSTRACT

Mo-Si-B silicides consisting of the phases  $\alpha$ -Mo (Mo solid solution),  $\text{Mo}_3\text{Si}$ , and  $\text{Mo}_5\text{SiB}_2$  have melting points on the order of 2000°C and have potential as ultra-high temperature structural materials. Mo-Si-B alloys can be processed such that the  $\alpha$ -Mo is present in the form of isolated particles in a silicide matrix, or as a continuous matrix “cementing” individual silicide particles together. The latter microstructure is similar to that of WC-Co hard metals. This paper focuses on the relationship between the topology as well as scale of the microstructure of Mo-Mo<sub>3</sub>Si-Mo<sub>5</sub>SiB<sub>2</sub> alloys, and their creep strength and fracture toughness. For example, the creep strength of Mo-Si-B alloys is improved by reducing the  $\alpha$ -Mo volume fraction and by making the  $\alpha$ -Mo phase discontinuous. The fracture toughness is improved by increasing the  $\alpha$ -Mo volume fraction and by making the  $\alpha$ -Mo phase continuous. Room temperature stress intensity factors as high as 21 MPa m<sup>1/2</sup> were obtained. The room temperature fracture toughness of Mo-Si-B alloys can also be improved by microalloying with Zr. The room temperature ductility of Mo itself can be improved by adding MgAl<sub>2</sub>O<sub>4</sub> spinel particles suggesting yet another way to improve the ductile phase toughening of Mo-Si-B alloys.

## INTRODUCTION

Nickel-base superalloys have outstanding oxidation and mechanical properties at elevated temperatures, but their service temperatures are inherently limited to temperatures around 1000°C. Oxide dispersion strengthened materials, with solidus temperatures as high as 1480°C [1], can operate above 1000°C. However, their creep strengths are relatively low. For example, the nickel-base ODS alloy MA754 has a 1000 h rupture strength of 78 MPa at 1150°C and the iron-base ODS alloy MA956 has a 100 h rupture strength of 51 MPa at 1100°C [1]. Also, these ODS alloys have high stress exponents which makes them prone to catastrophic fracture in creep since a small increase in stress can result in a dramatic increase in the creep rate. In order to increase the thermodynamic efficiency of fossil energy systems, strong, tough and oxidation resistant materials capable of service temperatures much higher than 1000°C are needed. While refractory elements such as Nb, Mo, Ta, and W have very high melting points, they lack oxidation resistance. One way to improve their oxidation resistance is to form silicides. A prime example is MoSi<sub>2</sub> that is widely used in heating

elements for resistance furnaces. Its good oxidation resistance is due to the formation of a protective silica glass scale. However,  $\text{MoSi}_2$  is very brittle with a room temperature fracture toughness on the order of  $3 \text{ MPa m}^{1/2}$  [2]. Also, it is very weak at high temperatures [2]. If the Si concentration is reduced below that of  $\text{MoSi}_2$ , phases such as  $\text{Mo}_5\text{Si}_3$ ,  $\text{Mo}_3\text{Si}$ , and  $\alpha\text{-Mo}$  (Mo solid solution) form. These phases will have a lower oxidation resistance, but their fracture toughness may be higher. As indicated in the schematic ternary phase diagram in Fig. 1, two main alloy systems have been examined to date. In the first one, which was pioneered by Akinc and collaborators [3-5], intermetallic alloys consisting of  $\text{Mo}_5\text{Si}_3$ , the T2 phase  $\text{Mo}_5\text{SiB}_2$ , and the A15 phase  $\text{Mo}_3\text{Si}$  were investigated. They exhibit excellent oxidation resistance at elevated temperatures (e.g.,  $1300^\circ\text{C}$ ). The boron additions are crucial for providing the observed oxidation resistance [4,5], as already hinted at in an early study of the ternary Mo-Si-B phase diagram by Nowotny et al. [6]. The second system is the focus of this paper and was pioneered by Berczik et al. [7,8]. Berczik investigated alloys consisting of  $\alpha\text{-Mo}$ ,  $\text{Mo}_3\text{Si}$ , and T2. While these alloys are not as oxidation resistant as  $\text{Mo}_5\text{Si}_3\text{-T2-Mo}_3\text{Si}$  alloys, they contain a ductile phase,  $\alpha\text{-Mo}$ . Depending on its volume fraction and distribution, the  $\alpha\text{-Mo}$  can improve the room and high temperature fracture toughness significantly. The fracture toughness increases with increasing  $\alpha\text{-Mo}$  volume fraction. For a given  $\alpha\text{-Mo}$  volume fraction, the fracture toughness is expected to be higher if the  $\alpha\text{-Mo}$  forms a continuous matrix instead of individual particles [9]. The fracture toughness is also expected to increase if the microstructural scale of the  $\alpha\text{-Mo}$  increases [10]. The oxidation resistance, on the other hand, is increased by decreasing the  $\alpha\text{-Mo}$  volume fraction and by distributing the  $\alpha\text{-Mo}$  in the form of isolated particles, instead of a continuous matrix. Clearly, then, the optimization of Mo- $\text{Mo}_3\text{Si}$ -T2 alloys requires a trade-off between fracture toughness on the one hand, and oxidation resistance on the other.

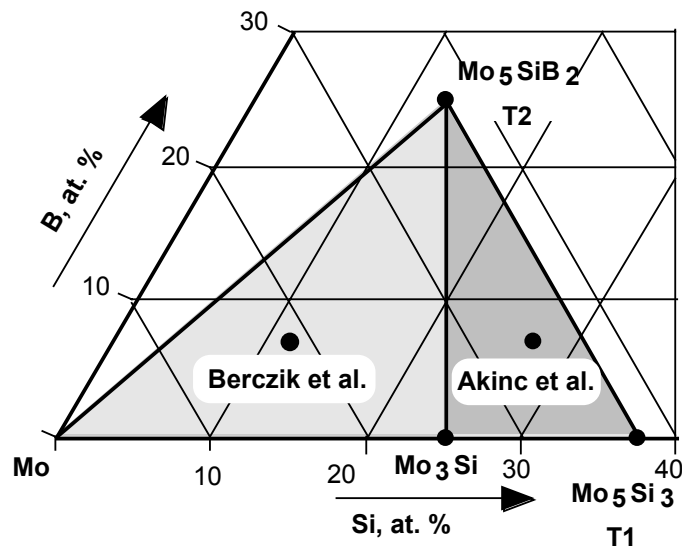


Figure 1: Schematic illustration of the Mo-rich section of the ternary Mo-Si-B phase diagram.

The creep resistance of Mo-Mo<sub>3</sub>Si-T2 alloys is governed by several factors. Mo<sub>3</sub>Si and Mo<sub>5</sub>SiB<sub>2</sub> are all very strong at elevated temperatures [11-13]. Since it can be safely assumed that the creep strength of  $\alpha$ -Mo is lower than that of Mo<sub>3</sub>Si and T2, the creep strength of Mo-Mo<sub>3</sub>Si-T2 alloys is likely to decrease as the  $\alpha$ -Mo volume fraction increases. The creep strength will also depend on the microstructural morphology - if the  $\alpha$ -Mo is distributed as a continuous matrix or “binder” phase instead of isolated particles, the creep strength may be relatively low. However, the microstructural scale is also important. By way of example, nickel-base superalloys consist of narrow (100 nm)  $\gamma$  solid solution channels between  $\gamma'$  (Ni<sub>3</sub>Al) particles. Their creep strength is determined by dislocation motion in the channels. It may therefore be beneficial for the creep strength of Mo-Mo<sub>3</sub>Si-T2 intermetallics if the continuous  $\alpha$ -Mo “channels” are very narrow, e.g., 100 nm. Such narrow channels might also be beneficial for room temperature toughening. Many bcc materials such as Mo or FeAl tend to fracture in a relatively brittle manner by cleavage. However, if the size scale of the FeAl phase is small enough, e.g., on the order of 1  $\mu$ m, ductile failure is observed in FeAl/TiC composites [14]. This is because the dislocation pile-ups in the FeAl ligaments cannot become long enough to nucleate cleavage fracture. Molybdenum ligaments in Mo-Mo<sub>3</sub>Si-T2 materials may behave in the same manner if they are sufficiently thin.

This introduction shows that many different factors need to be considered in the design of Mo-Mo<sub>3</sub>Si-T2 intermetallics. While oxidation resistance is a very important factor in their design, this particular paper will focus exclusively on the design of the mechanical properties by controlling the scale and topology of the microstructure, as well as by improving the mechanical properties of the toughening  $\alpha$ -Mo phase.

## EXPERIMENTAL

The alloys in this work were prepared by arc-melting of elemental starting materials in a partial pressure of argon (70 kPa) on a water-cooled copper hearth. The purity of the starting materials Mo, Si and B was 99.95, 99.99, and 99.5 weight % (wt%), respectively. Some alloys were microalloyed with high-purity Ti or Zr. Unless stated otherwise, alloy compositions will be stated in atomic % (at. %). The alloys were re-melted several times in order to improve their homogeneity. Some alloys were drop-cast into cylindrical water-cooled copper molds with diameters of 12.5 or 25 mm. When the alloys were examined in the cast and annealed condition, their annealing treatment was 24 hours at 1600°C in vacuum at a pressure of approximately 10<sup>-4</sup> Pa. Several as-cast alloys were crushed into powders with sizes ranging from <50 to 230  $\mu$ m. In a recently developed approach, the surfaces of the crushed Mo-Si-B powders were “coated” with a thin (e.g., 10  $\mu$ m) layer of Mo by removing Si via vacuum annealing [15]. The powders were consolidated by hot isostatic pressing (HIPing) in evacuated Nb cans. The HIPing conditions were 4h at a temperature of 1600°C and a pressure of 200 MPa.

Metallography specimens were prepared by grinding, mechanical polishing, and etching in Murakami’s reagent. Microstructural examination was carried out by optical microscopy as well as scanning electron microscopy (SEM). The phases were identified by a combination of energy dispersive spectroscopy (EDS) in an SEM, by wavelength-dispersive spectroscopy (microprobe), and powder x-ray diffraction. Images were typically obtained in the backscattered electron (BSE) mode in order to maximize the contrast between the different phases.

Compression specimens with a diameter of 3 mm and a height of 6 mm were electro-discharge machined. Their creep strengths were evaluated from constant displacement rate tests with an initial strain rate of  $10^{-5} \text{ s}^{-1}$  in flowing argon at  $1300^\circ\text{C}$  in an Instron testing machine equipped with a  $\text{MoSi}_2$  furnace. Button-head tensile specimens with gage diameters and lengths of 3.2 and 12.5 mm, respectively, were machined by grinding to a #8 finish.

For the purpose of screening tests, the fracture toughness  $K_q$  was determined from flexure tests with chevron-notched flexure bars with a cross-section of  $3 \times 4 \text{ mm}$  and a span of 20 mm (see also Fig. 2):

$$K_q = [EG/(1-\nu^2)]^{1/2}, \quad (1)$$

where  $E$  is Young's modulus,  $G=W/A$  is the work  $W$  expended during fracture divided by the area  $A$  swept out by the crack, and  $\nu$  = Poisson's ratio. The fracture toughness values determined with this technique tend to be higher than those determined with more rigorous techniques. On the other hand, this technique is very simple to implement and is suitable for comparative purposes.

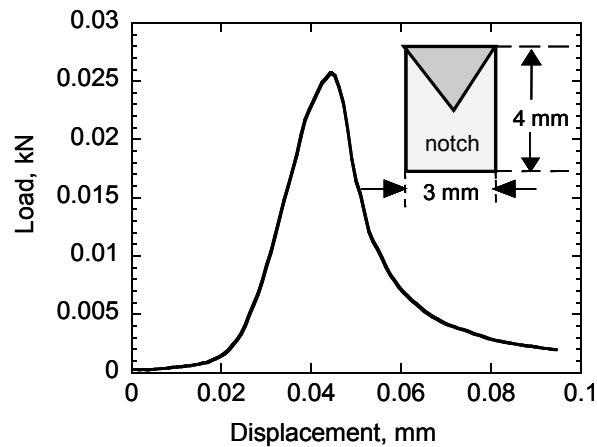


Figure 2. Determination of  $K_q$  from flexure tests with chevron-notched flexure bars

Precise fracture toughness values were obtained under plane-strain conditions by monotonically loading fatigue-precracked, disk-shaped compact-tension DC(T) specimens to failure. During these tests, crack lengths were periodically monitored using the elastic unloading compliance. Following pre-cracking, specimens were cycled for  $\sim 24$  hr at the  $\Delta K_{TH}$  threshold (where there is no discernable crack growth) in an attempt to remove any possible crack bridging in the wake of the pre-crack. The resistance curve (R-curve) behavior was then evaluated by measuring the crack-growth resistance,  $K_R$ , as a function of crack extension,  $\Delta a$ .

## RESULTS AND DISCUSSION

### MICROSTRUCTURES

Figure 3 shows an SEM micrograph of cast and annealed Mo-12Si-8.5B. The  $\alpha$ -Mo (bright) has a volume fraction on the order of 40% and appears to be discontinuous.

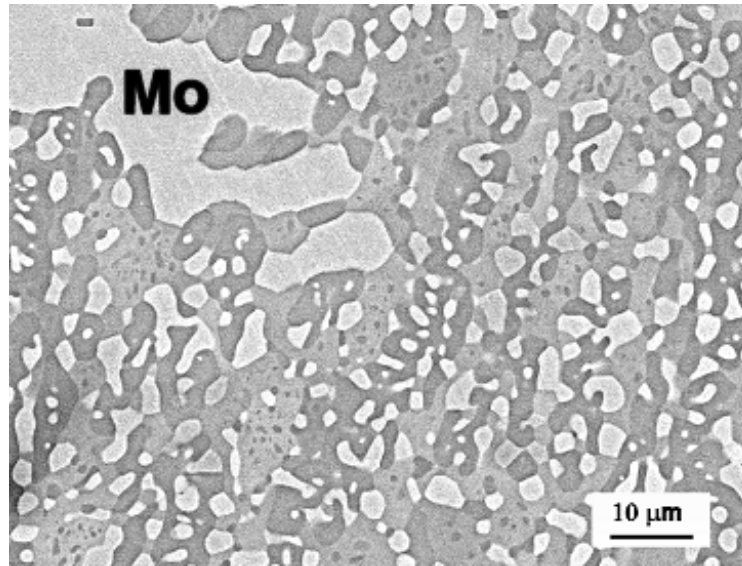


Figure 3. Cast and annealed Mo-12Si-8.5B. The bright particulate phase is  $\alpha$ -Mo.

Table I lists the initial powder sizes and the  $\alpha$ -Mo volume fraction of four silicide alloys fabricated from Mo-20Si-10B ( $\text{Mo}_3\text{Si}/\text{T}_2$ ) powders by the Si evaporation/HIPing technique [15]. SEM images of the microstructures of the alloys are shown in Fig. 4. In comparing these pictures, it should be kept in mind that their scale markers are different.

Table I. Mo- $\text{Mo}_3\text{Si}$ -T<sub>2</sub> alloys fabricated by the Si evaporation technique [15].

Specimen Designation	Powder size prior to Si removal	$\alpha$ -Mo volume fraction, %
fine	$\leq 45 \mu\text{m}$	34
medium	45-90 $\mu\text{m}$	34
coarse	90-180 $\mu\text{m}$	49
medium-low	45-90 $\mu\text{m}$	5

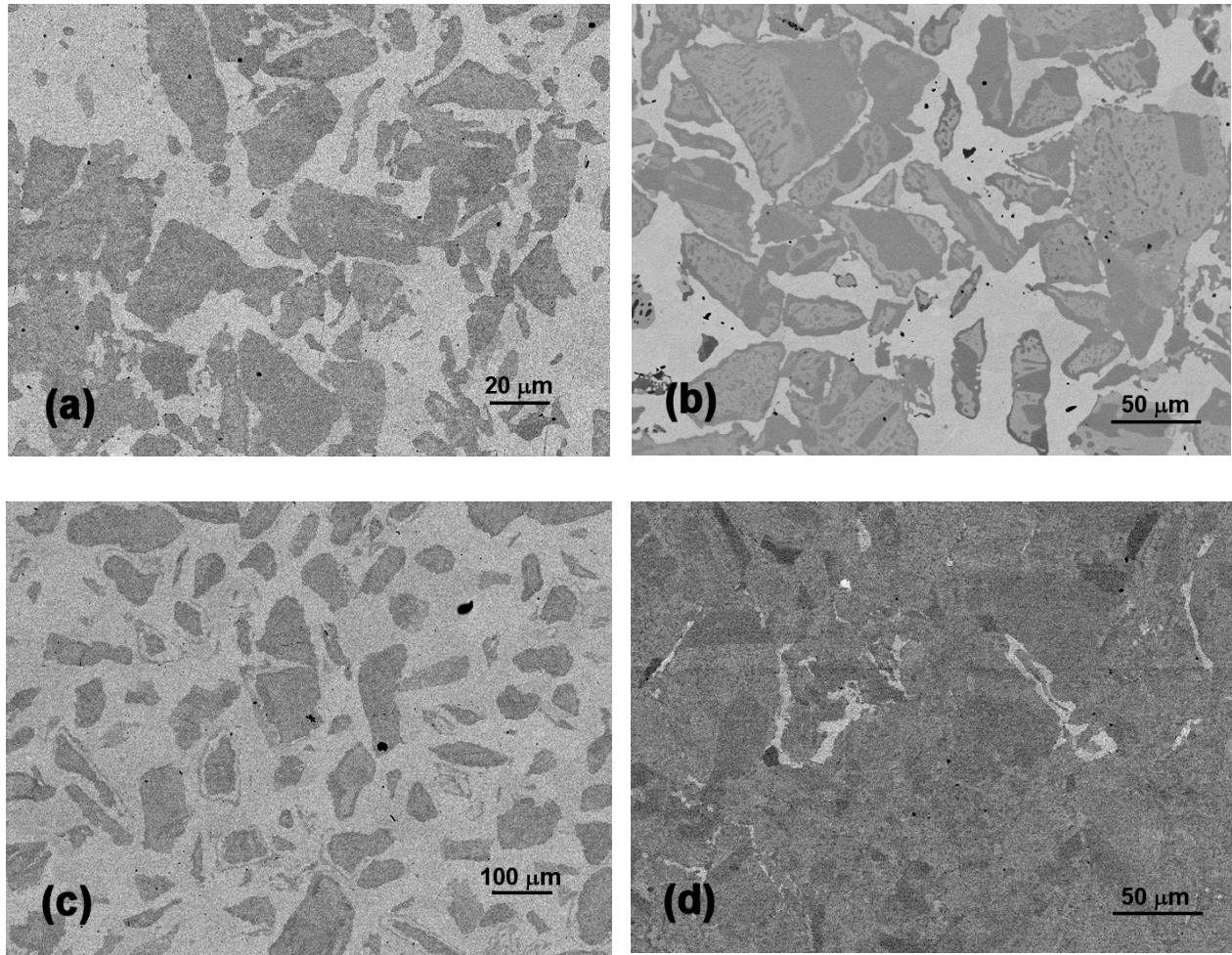


Figure 4. BSE-SEM micrographs of the Mo-Si-B alloys listed in Table I: (a) “fine”, (b) “medium”, (c) “coarse” and (d) “medium-low.”

#### TENSILE STRENGTH AND CREEP STRENGTH

A specimen with the “coarse” microstructure was tested in tension at room temperature. It failed prematurely in a brittle manner at a stress of 140 MPa. At 1200°C in vacuum and an initial strain rate of  $3.3 \times 10^{-3} \text{ s}^{-1}$ , the 0.2% yield stress was 336 MPa, the maximum stress 354 MPa, and the ductility 1.8%. The low ductility value suggests that the mechanical properties of the  $\alpha$ -Mo matrix need to be improved further.

Figure 5 compares the creep strength of cast and annealed Mo-12Si-8.5B with that of the four powder-metallurgically processed alloys. The trends in the data are interpreted as follows. The cast and annealed alloy has the highest creep strength since it exhibits a continuous matrix of strong  $\text{Mo}_3\text{Si}/\text{T}_2$ . The “fine” alloy is much weaker because of its fine-scale microstructure and the relatively weak continuous  $\alpha$ -Mo matrix. Coarsening the microstructure, while keeping the volume fraction constant, improves the creep strength (“medium”). Reducing the  $\alpha$ -Mo volume fraction to 5% increases

the creep strength only slightly. This result is not well understood since the  $\alpha$ -Mo in this alloy (“medium-low”) appears to be discontinuous (Fig. 3(d)). One would therefore expect the creep strength to be higher than that of the cast and annealed alloy with 40 vol.%  $\alpha$ -Mo. Finally, the “coarse” alloy is much weaker than any of the other alloys. This is to be expected in view of its high volume fraction of continuous  $\alpha$ -Mo.

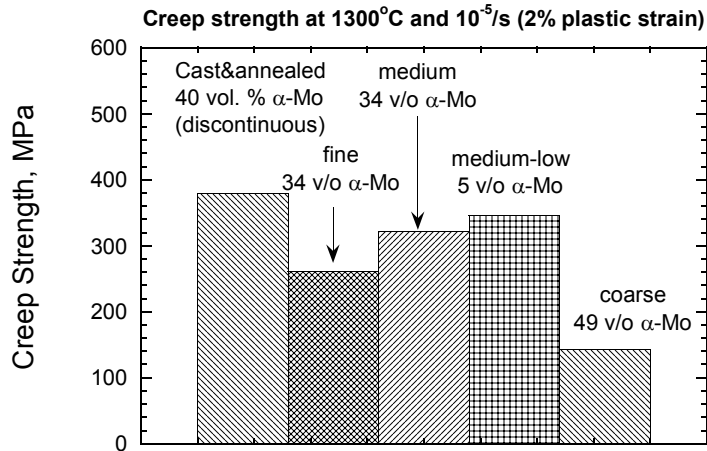


Figure 5. Creep strength of Mo-Si-B alloys at 1300°C and an initial strain rate of  $10^{-5} \text{ s}^{-1}$  for different microstructural topologies, scales, and  $\alpha$ -Mo volume fractions.

## FRACTURE TOUGHNESS

Figure 6 compares the room temperature R-curves for several Mo-Si-B materials. Cast&annealed Mo-Si-B with an  $\alpha$ -Mo volume fraction of approximately 40 vol.% shows only a small increase in crack growth resistance with crack extension. More pronounced R-curve behavior is found for a volume fraction of 34% of continuous  $\alpha$ -Mo. This suggests that continuous  $\alpha$ -Mo is more effective in providing extrinsic toughening (i.e., crack tip shielding by bridging in the wake of the crack) than discontinuous  $\alpha$ -Mo. Finally, when the  $\alpha$ -Mo volume fraction is increased to 49%, a high value of the initiation toughness,  $12 \text{ MPa m}^{1/2}$ , and pronounced R-curve behavior are observed. The stress intensity factor reaches a value as high as  $21 \text{ MPa m}^{1/2}$ . This shows clearly that Mo-Si-B alloys with high fracture toughness can be designed.

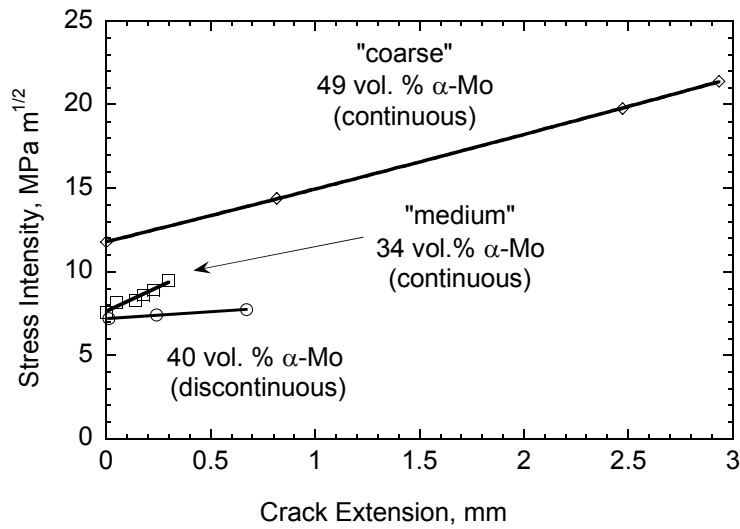


Figure 6. Room temperature crack growth resistance of Mo-Si-B alloys

As pointed out in the introduction, efforts to further increase the fracture toughness (or to maintain a certain value of the fracture toughness while reducing the  $\alpha$ -Mo volume fraction) must focus on the mechanical properties of the  $\alpha$ -Mo phase. It is well known that microalloying additions of Zr and Ti improve the mechanical properties of Mo alloys. The best-known example is TZM (Mo-0.5Ti-0.1Zr, wt%). Table II lists the fracture toughness values of cast and annealed Mo-Si-B alloys in which Mo was partially substituted with Ti or Zr. Note that these  $K_q$  values are only suitable for comparative purposes. Table II shows that small additions of Zr (1.5 at. %) do improve the fracture toughness of Mo-Mo<sub>3</sub>Si-T2 alloys. Since it is considered unlikely that the Zr addition improves the fracture toughness of Mo<sub>3</sub>Si and T2, Zr acts presumably by improving the mechanical properties of the toughening  $\alpha$ -Mo phase.

Table II. Fracture toughness  $K_q$  of Mo-Si-B alloys micro-alloyed with Ti or Zr.  $K_q$  was evaluated from eqn. (1) assuming  $E=327$  GPa and  $\nu=0.29$ .

	Area of triangle broken during test, mm <sup>2</sup>	Absorbed energy, mJ	G, J/m <sup>2</sup>	$K_q$ , MPa m <sup>1/2</sup>	$K_q$ , MPa m <sup>1/2</sup> , average±standard deviation
Mo-12Si-8.5B	2.94	0.68	231	9.1	
“	2.88	0.775	267	9.8	9.0±0.8
“	3.19	0.603	189	8.2	
Mo-12Si-8.5B-1.5Ti	2.86	0.905	317	10.6	10.0±0.8
“	2.81	0.692	246	9.4	
Mo-12Si-8.5B-1.5Zr	3.05	1.575	516	13.6	
“	3.48	1.93	555	14.1	13.5±0.7
“	2.89	1.32	457	12.8	



In the 1960's, Scruggs found that powder-metallurgical Cr is ductilized by addition of MgO particles that transform into  $\text{MgCr}_2\text{O}_4$  spinel particles [16]. Under the Fossil Energy Materials Program, M. P. Brady verified this ductilizing effect [17]. He determined that segregation of detrimental impurities such as nitrogen to the particle-matrix interface is one of the factors responsible for ductilization. Scruggs found that Mo can also be ductilized by adding spinel particles [18]. Nominally pure Mo and Mo-3.4 wt%  $\text{MgAl}_2\text{O}_4$  coupons were prepared by hot-pressing at 1800°C. Figure 7 qualitatively compares their bend ductility. Clearly, the addition of the spinel particles improves the ductility substantially. If Mo-Si-B intermetallics with an  $\alpha$ -Mo phase containing spinel particles could be produced, their fracture toughness would be increased due to the increased ductility of the  $\alpha$ -Mo phase. It is presently not clear how such a microstructure could be produced. Also, it is not known what particle size and volume fraction would provide the highest ductility increase.

In order to attain satisfactory oxidation resistance, the  $\alpha$ -Mo volume fraction in Mo-Si-B intermetallics has to be kept as low as possible. This, in turn, means that the mechanical properties of the  $\alpha$ -Mo have to be improved as much as possible. Microalloying with Zr and adding spinel dispersoids present two possible options to achieve that aim.

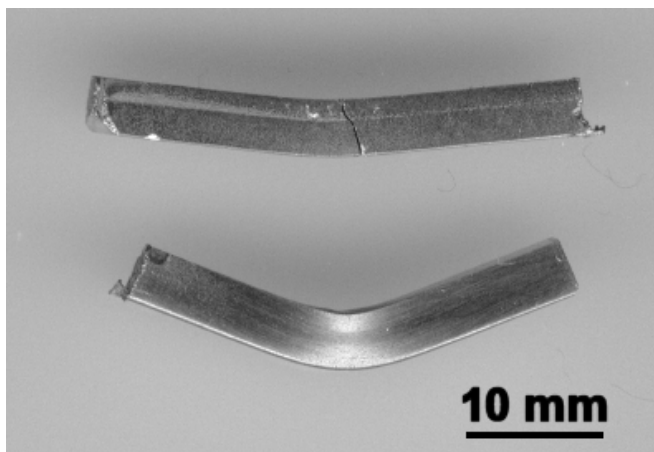


Figure 7. Qualitative comparison of the room temperature bend ductility of Mo and Mo-3.4 wt%  $\text{MgAl}_2\text{O}_4$ .

## CONCLUSIONS

Mo-Si-B intermetallics can be processed such that the  $\alpha$ -Mo occurs either in the form of discrete particles or as a continuous matrix. The creep strength is seen to depend on the microstructural topology and scale, as well as the  $\alpha$ -Mo volume fraction. With 49 vol.% of continuous  $\alpha$ -Mo, very high fracture toughness values up to  $21 \text{ MPa m}^{1/2}$  can be obtained. It is considered very important to further improve the mechanical properties of the  $\alpha$ -Mo phase. This will increase its efficiency for providing toughening. In order to achieve a certain value of the fracture toughness, less  $\alpha$ -Mo will then be required, with a concomitant improvement in the oxidation resistance. The mechanical properties of  $\alpha$ -Mo can be improved by micro-alloying with Zr or by dispersing  $\text{MgAl}_2\text{O}_4$  spinel particles. Future work will examine issues such as the optimum size and volume fraction of the spinel particles and ways to incorporate them in the  $\alpha$ -Mo phase of three-phase Mo-Mo<sub>3</sub>Si-Mo<sub>5</sub>SiB<sub>2</sub> silicides.

## ACKNOWLEDGEMENTS

This work was sponsored by the Office of Fossil Energy, Advanced Research Materials (ARM) Program, U.S. Department of Energy, under contract DE-AC05-00OR22725 with Oak Ridge National Laboratory managed by UT-Battelle, LLC. The work of J. J. Kruzic and R. O. Ritchie was supported by the Director, Office of Science, Office of Basic Energy Sciences, Division of Materials Sciences and Engineering of the U.S. Department of Energy under contract No. DE-AC03-76SF00098 with the Lawrence Berkeley National Laboratory and the multi-National Laboratory program on "Design and Synthesis of Ultrahigh-Temperature Intermetallics" within the DOE Center for Excellence and Processing of Advanced Materials.

## REFERENCES

1. www.specialtymetals.com.
2. A. K. Vasudévan and J. Petrovic, "A comparative overview of molybdenum silicide composites," *Mater. Sci. and Engng.* A155 (1992) 1-17.
3. M. K. Meyer, M. J. Kramer, and M. Akinca [sic], "Compressive creep behavior of  $\text{Mo}_5\text{Si}_3$  with the addition of boron," *Intermetallics* 4 (1996) 273-281.
4. M. Akinc, M. K. Meyer, M. J. Kramer, A. J. Thom, J. J. Huebsch, and B. Cook, "Boron-doped molybdenum silicides for structural applications," *Intermetallics* A261 (1999) 16-23.
5. M. K. Meyer, A. J. Thom, and M. Akinc, "Oxide scale formation and isothermal oxidation behavior of Mo-Si-B intermetallics at 600-1000°C," *Intermetallics* 7 (1999) 153-162.
6. H. Nowotny, E. Dimakopoulou, and H. Kudielka, "Untersuchungen in den Dreistoffsystemen: Molybdän-Silizium-Bor, Wolfram-Silizium-Bor und in dem System:  $\text{VSi}_2$ - $\text{TaSi}_2$ ," *Mh. Chem.* 88 (1957) 180-192.
7. D. M. Berczik, United States Patent 5,595,616 (1997), "Method for enhancing the oxidation resistance of a molybdenum alloy, and a method of making a molybdenum alloy."
8. D. M. Berczik, United States Patent 5,693,156 (1997), "Oxidation Resistant Molybdenum Alloys."
9. R. Raj and L. R. Thompson, "Design of the microstructural scale for optimum toughening in metallic composites," *Acta Metall. Mater.* 42 (1994) 4135-4142.
10. M. F. Ashby, F. J. Blunt, and M. Bannister, "Flow Characteristics of highly constrained Metal Wires," *Acta Metall.*, 37[7] (1989) 1847-1857.
11. I. Rosales and J. H. Schneibel, "Stoichiometry and mechanical properties of  $\text{Mo}_3\text{Si}$ ," *Intermetallics* 8 (2000) 885-889.
12. K. Ito, K. Ihara, K. Tanaka, M. Fujikura, M. Yamaguchi, "Physical and mechanical properties of single crystals of the T2 phase in the Mo-Si-B system," *Intermetallics* 9[7] 591-602 (2001).
13. R. D. Field, D. J. Thoma, J. C. Cooley, F. Chu, C. L. Fu, M. H. Yoo, W. L. Hulst, C. M. Cady, "Dislocations in  $\text{Mo}_5\text{SiB}_2$  T2 Phase," *Intermetallics* 9 (2001) 863-868
14. R. Subramanian and J. H. Schneibel, "The Ductile-Brittle Size Transition of Iron Aluminide Ligaments in an FeAl/TiC Composite," *Acta Materialia*, 46[13] (1998) 4733-4741.

15. J.H. Schneibel, M.J. Kramer, and D.S. Easton, "A Mo-Si-B intermetallic alloy with a continuous  $\alpha$ -Mo matrix," *Scripta Materialia* 46 (3) (2002) pp. 217-221.
16. D. M. Scruggs, L. H. Van Vlack, and W. M. Spurgeon, *J. Amer. Ceram.Soc.* 51 (1968) 473.
17. M. P. Brady, I. M. Anderson, M. L. Weaver, H. M. Meyer, L. R. Walker, M. K. Miller, D. J. Larson, I. G. Wright, V. K. Sikka, a. Rar, G. M. Pharr, J. R. Keiser, and C. A. Walls, "Nitrogen impurity gettering in oxide dispersion ductilized chromium," accepted for publication in *Materials Science and Engineering A*.
18. D. M. Scruggs, "Ductile tungsten composition containing a spinel dispersed uniformly throughout," United States Patent 3,320,037, Patented May 16, 1967.